Silver, E. A., Rangin, C., von Breymann, M. T., et al., 1991
Proceedings of the Ocean Drilling Program, Scientific Results, Vol. 124

7. ELECTRICAL PROPERTIES OF BASALTS FROM SITES 768 AND 770[1]

Richard D. Jarrard[2] and Ralph Schaar[2]

ABSTRACT

Conductivity of 54 basalt samples from ODP Sites 768 and 770 was measured as a function of temperature and fluid salinity. Porosity was also measured for all samples, and cation exchange capacity was measured for 46 of the samples. Porosity measurements indicated that porosity is underestimated for basalts like these, unless one uses extensive drying at high vacuum.

At salinities greater than 29 ppt, and throughout the range of salinity and temperatures likely *in situ*, sample conductivity (C_o) is controlled by porosity (ϕ) according to the Archie relation $C_o = 0.22 \cdot C_w \cdot \phi^{1.3}$ *(or* $FF = 4.5/f1.3$*)*, where Cw is conductivity of the pore fluids and $FF = C_w/C_o$ is the formation factor. At lower salinity, clay-surface conduction or microcrack conduction may dominate. We are unable to distinguish reliably between the two mechanisms, but we do detect their effects subtly at high salinity and strongly at low salinity.

INTRODUCTION

Electrical properties of basalts may provide clues to the aging of oceanic crust. According to the standard model for hydrologic aging, newly created crust is very hot, very porous, and very permeable, with porosity composed primarily of microcracks and secondarily of vesicles and fractures. Accordingly, hydrothermal circulation is vigorous at spreading centers. Associated with this hydrothermal activity is mass flux into and out of the formation, resulting in black smokers on the seafloor and alteration of the top 1 km or more of crust. As the crust ages, velocities and densities increase while porosities and permeabilities decrease and magnetic minerals oxidize, until hydrothermal circulation is greatly attenuated. The electrical properties of oceanic basalts are sensitive to both porosity and clay alteration minerals; these properties are therefore a potentially sensitive barometer of crustal aging.

ODP Leg 124 cored 106 m of basaltic crust at Site 770 in the Celebes Sea and 222 m of basaltic crust at Site 768 in the Sulu Sea (Rangin, Silver et al., 1990). Based on trace-element geochemistry and other data, the basalts at Site 770 are mid-ocean ridge basalts (MORB), formed in the middle Eocene, probably at a moderate spreading rate of about 28–45 mm/yr (Weissel, 1980), and apparently later trapped as the Celebes Sea by microplate reorganization (Rangin, Silver et al., 1990). In contrast, the basalts at Site 768 formed by back-arc spreading in the early middle Miocene. Complete suites of *in- situ* geophysical logs were obtained through both basalt intervals; these logs included velocity, density, neutron porosity, resistivity, and three-component magnetometer. The 222 m of basaltic penetration at Site 768 is the deepest ever into crust of back-arc origin, and the only significant amount of back-arc crust ever logged. The 106 m of crust logged at Site 770 surpasses all but a handful of DSDP and ODP sites and partially bridges the major gap between 6- and 110-Ma *in-situ* measurements of the geophysical properties of oceanic crust.

This project examines the physical properties and geophysical indications of alteration in core samples from the two sites, to establish the interrelations of resistivity, primary porosity, alteration, and velocity. Here we focus on the electrical properties of core samples, because the electrical properties of oceanic basalts are particularly sensitive to the magnitude and geometry of porosity and possibly also to amount of authigenic clays. In a companion paper, we use these core data as a calibration of some geophysical properties of downhole logs at the two sites.

METHODS

A total of 54 basalt samples were obtained from Sites 768 and 770. We deliberately confined our measurements to all available samples with shipboard measurements of velocity, porosity, bulk density, and grain density (Table 1); shipboard measurement techniques are described by Shipboard Scientific Party (1990). Virtually all samples were 1-in. cylinders, drilled into the working half such that the long axis of each cylinder (and our resistivity measurement direction) corresponds to a horizontal *in-situ* orientation. Almost all cylinders were flattened with a diamond saw on board the ship, so that vertical compressional-wave velocities could be measured. Six samples from Site 768 were exceptions: they were quarter rounds, with both shipboard velocity and our resistivity measured vertically and with no shipboard measurements of porosity, bulk density, and grain density. The dimensions of all samples were measured, for conversion of measured resistances to resistivities.

Upon examining the shipboard measurements on these samples, we suspected that the freeze-drying procedure utilized did not drive all pore waters from microcracks. This suspicion was based on the strong inverse correlation between porosity and grain density, with many very low grain densities of less than 2.65. Therefore we remeasured these index properties as follows. We first removed most residual sea salt by evacuating the samples at low vacuum and room temperature, in a vacuum oven. We then saturated them with distilled water by dropping them into the fluid and removing the vacuum. Samples were then dried for 7 days in the low-vacuum (approx. 0.1 atmosphere) vacuum oven, with two interruptions for intermediate weighings and a weighing at the end. Finally, samples were dried further for 2.9 days at very high vacuum (150–200 mm), then weighed. The samples were

[1] Silver, E. A., Rangin, C., and von Breymann, M. T., et al., 1991. *Proc. ODP, Sci. Results,* 124: College Station, TX (Ocean Drilling Program).

[2]Lamont-Doherty Geological Observatory of Columbia University, Palisades, NY 10964, U.S.A.

Table 1. Index properties for basalts from Leg 124 Sites 768 and 770.

		Rangin, Silver et al., 1990				this study		
Sample location	mbsf	Bulk density[a]	Grain density[a]	Porosity[a]	Velocity[a]	Bulk density[b]	Grain density[b]	Porosity[b]
768-74-2, 37	1058.12	2.40	2.66	19.9	3.27	2.34	2.73	22.6
768-75-2, 45	1067.85	2.44	2.74	26.1	3.18			
768-76-1, 134	1076.94	2.45	2.76	25.8				
768-77-2, 52	1082.56	2.81	2.94	30.2				
768-78-1, 27	1085.87	2.33	2.61	20.7	3.18	2.29	2.72	25.0
768-79-1, 38	1090.98	2.35	2.62	21.7	3.25	2.31	2.73	24.6
768-80-1, 77	1096.37	2.32	2.60	22.4	3.19	2.24	2.65	25.5
768-81-1, 19	1100.79	2.32	2.60	23.6	3.11	2.26	2.68	25.3
768-82-2, 17	1107.22	2.32	2.61	23.5	3.31	2.33	2.74	24.2
768-83-1, 137	1111.97	2.35	2.84	10.3	3.20	2.22	2.67	27.7
768-84-2, 93	1118.03	2.37	2.57	18.4	3.37	2.29	2.65	22.1
768-85-1, 37	1120.97	2.50	2.67	9.6	3.04			
768-86-1, 46	1127.06	2.55	2.79	25.7	3.35			
768-87-1, 37	1136.67	2.48	2.67	21.8				
768-88-1, 28	1146.28	2.47	2.62	14.6	3.75	2.37	2.66	17.7
768-88-2, 114	1148.46	2.58	2.79	3.9	4.11	2.52	2.78	14.5
768-89-1, 77	1156.47	2.77	2.81	17.2	4.28	2.60	2.81	11.8
768-89-2, 5	1157.25	2.60	2.65	0.7	4.56	2.51	2.68	10.6
768-89-4, 50	1160.12	2.75	2.74	5.4	5.00	2.65	2.79	7.7
768-90-2, 59	1167.20	2.66	2.76	8.7	4.11	2.59	2.78	10.5
768-90-3, 50	1168.41	2.81	2.76	13.5	4.69	2.66	2.79	7.2
768-90-5, 72	1171.49	2.83	2.77	11.6	4.92	2.70	2.79	5.6
768-90-7, 104	1174.12	2.82	2.74	12.2	4.99	2.70	2.82	6.5
768-91-1, 32	1175.22	2.74	2.74	4.5	5.15	2.71	2.81	5.7
768-92-2, 22	1186.17	2.78	2.80	3.4	4.88	2.69	2.79	5.5
768-92-3, 135	1188.55	2.75	2.76	3.8	4.90	2.68	2.78	5.3
768-93-3, 60	1195.05	2.59	2.71	14.1				
768-94-1, 90	1201.60	2.62	2.72	10.3				
768-95-1, 24	1210.64	2.50	2.75	20.9				
768-96-3, 126	1224.13	2.67	2.76	11.5				
768-97-3, 46	1232.92	2.68	2.65	8.0				
768-98-1, 48	1239.88	2.31	2.62	17.8		2.27	2.69	25.3
768-98-2, 54	1241.44	2.43	2.60	10.1	4.32	2.35	2.57	14.7
768-99-3, 98	1252.92	2.40	2.68	20.3		2.32	2.72	24.0
768-100-1, 36	1259.16	2.36	2.44	12.6	3.41	2.22	2.55	21.7
768-74-1, 115	1057.45				3.46	2.39	2.76	21.5
768-77-1, 48	1081.08				3.11	2.17	2.62	28.3
768-93-2, 12	1193.12				4.62	2.62	2.77	8.8
768-94-1, 76	1201.46				4.26			
768-95-1, 4	1210.44				3.54	2.40	2.76	21.1
768-96-1, 106	1221.06				3.52	2.25	2.69	26.3
768-97-3, 65	1233.11				4.90	2.41	2.60	12.2
770B-16-3,73	420.43	2.80	2.82	5.8	5.26			
770B-16-4, 26	421.41	2.86	2.85	1.7	5.72	2.78	2.83	2.5
770B-17-1, 22	426.02	2.80	2.80	4.2	5.50			
770B-17-3, 21	428.94	2.76	2.80	6.1	5.04			
770B-18-1, 57	436.17	2.83	2.83	3.1	5.23			
770B-18-2, 108	438.12	2.81	2.84	6.0	5.24			
770B-19-1, 96	446.06	2.22	2.74	3.3	4.70			
770B-19-2, 31	446.91	2.67	2.65	6.7	4.90			
770B-20-1, 27	455.07	2.45	2.65	18.1	4.02			
770B-20-2, 94	457.10	2.75	2.74	4.6	4.70			
770B-20-3, 12	457.62	2.81	2.79	3.4	5.60			
770B-20-4, 77	459.63	2.69	2.73	7.4	5.25			
770B-21-2, 91	466.84	2.76	2.78	4.8	5.14			
770B-21-4, 101	469.42	2.78	2.78	3.2	5.30			
770B-21-6, 93	472.08	2.78	2.79	3.8	5.25			
770-2-2, 80	425.47	2.84	2.85	4.0	5.17	2.80	2.91	5.8
770-3-2, 72	435.12	2.78	2.79	4.0	5.12	2.74	2.86	6.6
770-3-3, 23	436.13	2.70	2.78	7.4	4.69	2.62	2.80	10.3
770-3-4, 102	438.42	2.80	2.81	4.9	5.05	2.73	2.86	6.9
770-4-1, 29	442.89	2.82	2.80	1.8	5.42	2.76	2.82	2.9
770-4-3, 38	445.98	2.59	2.72	13.6	4.96			
770-5-1, 67	452.87	2.84	2.84	1.9	5.58	2.79	2.85	3.3
770-5-3, 40	454.96	2.82	2.81	2.6	5.39	2.79	2.86	3.9
770-5-4, 37	456.19	2.84	2.83	3.0	5.66	2.73	2.81	4.5
770-5-7, 27	460.21	2.82	2.83	2.6	5.42	2.74	2.81	4.0
770-6-1, 82	462.72	2.69	2.72	4.9	4.98	2.58	2.71	7.6
770-6-3, 116	465.90	2.78	2.80	3.6	5.42	2.77	2.87	5.0
770-6-1, 107	468.81	2.81	2.81	3.8	5.27	2.70	2.81	6.1
770-7-1, 27	471.77	2.64	2.67	6.0	5.01	2.54	2.67	8.3
770-7-3, 84	475.17	2.76	2.76	4.2	4.99	2.70	2.82	6.7
770-7-5, 107	478.21	2.86	2.84	1.8	5.76	2.82	2.89	4.0
770-9-2, 29	492.59	2.79	2.84	4.4	5.06	2.75	2.89	7.5
770-9-2, 120	493.50	2.81	2.81	3.0	5.21	2.75	2.84	5.1
770-10-1, 140	501.90	2.85	2.85	2.4	5.39	2.81	2.89	4.4
770-10-2, 9	502.09	2.88	2.87	2.6	5.37	2.79	2.89	5.1
770-10-3, 8	503.47	2.90	2.89	3.2	5.55	2.82	2.92	5.2
770-11-1, 93	511.11	2.79	2.80	3.9	5.08			
770-11-2, 99	512.52	2.86	2.85	3.3	5.30	2.80	2.90	5.1
770-12-1, 8	519.98	2.89	2.87	2.0	5.46	2.82	2.89	3.6
770-12-2, 66	522.06					2.80	2.87	3.7

[a]Rangin, Silver, von Brymann, et al., 1990.
[b]This study.

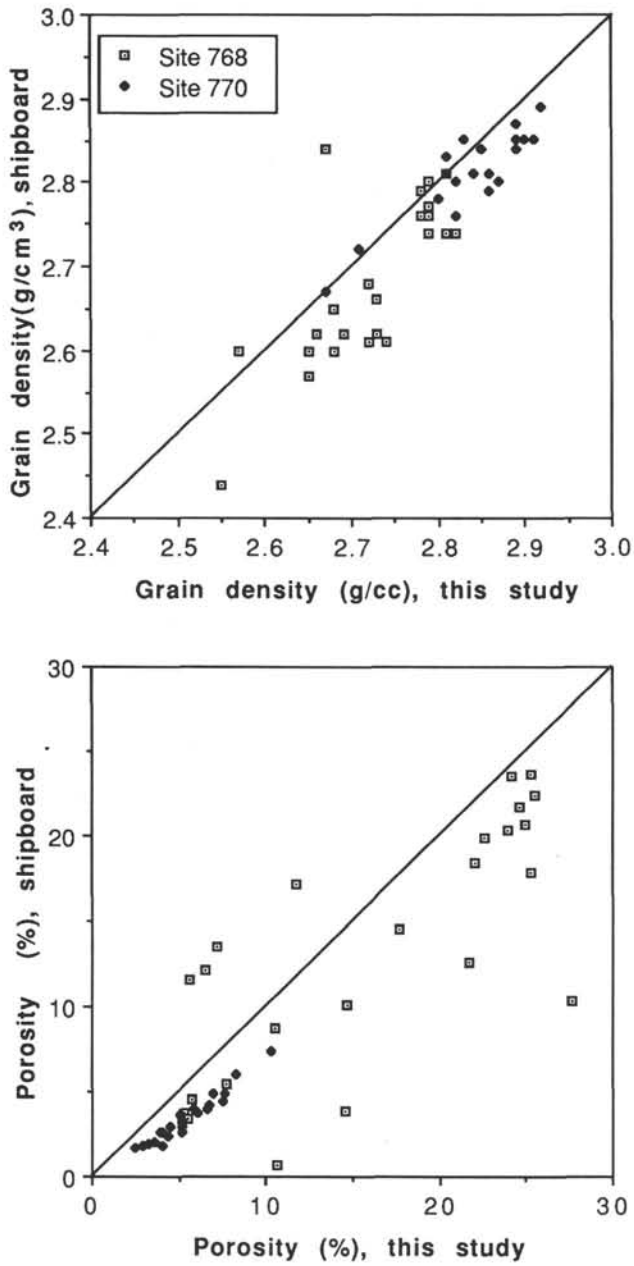

Figure 1. Comparison of our shore-based measurements of grain density and porosity to those made on the same basalt samples during ODP Leg 124. We attribute the lower grain densities and porosities of shipboard measurements to incomplete drying of samples.

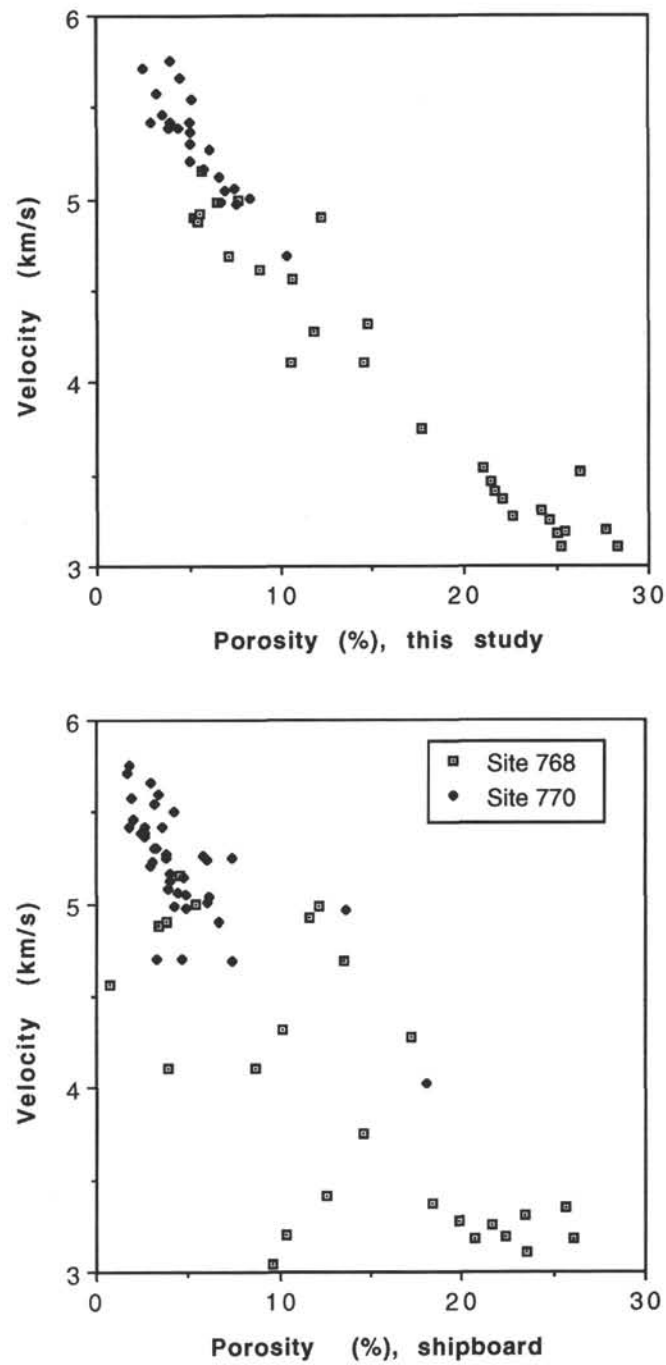

Figure 2. The relationship of compressional-wave velocity to porosity, in basalts of Sites 768 and 770. The upper figure yields a much closer relationship of velocity to porosity than does the lower figure, suggesting that the shore-based porosities determined in this study are more accurate than the shipboard porosities.

then "vacuum" saturated with artificial seawater (29.5 parts per thousand [ppt] sea salt), followed by weighing and measurement of wet volume by displacement.

The final drying in high vacuum caused a substantial weight loss, and our resulting grain densities and porosities (Table 1) are substantially higher than those obtained by Rangin, Silver, et al. (1990) or by us with only our drying in a commercial vacuum oven (Fig. 1). We consider these final index properties to be more reliable, and this conclusion is confirmed by the substantial improvement in correlation obtained between velocity and porosity (Fig. 2). Although these final porosities are the best available for comparison to subsequent resistivity measurements, it does not necessarily follow that we have succeeded in either driving out all water from partially sealed microcracks during drying or in fully resaturating the samples after drying. Indeed, these questions will be returned to later and will assume an important role in interpretations of resistivity measurements.

Resistivity measurements were made on saturated samples with a Genrad 1650B LCR Bridge, utilizing a 1-kHz, 50-mV alternating current and a two-electrode technique, at atmo-

Table 2. Conductivity measurements as a function of temperature and salinity at Leg 124 sites.

Sample		Conductivity (mS/m)											
		S=87.6	S=87.6	S=87.6	S=29.5	S=29.5	S=29.5	S=4.4	S=4.4	S=4.4	S=1.2	S=1.2	S=1.2
Sample Location	mbsf	T=10	T=25	T=50	T=10	T=25	T=50	T=10	T=25	T=50	T=10	T=25	T=50
768-74-1, 115	1057.45	316.2	471.6	788.7	143.8	218.9	374.7	95.3	150.3	273.8	59.4	113.5	250.0
768-74-2, 37	1058.12	219.2	317.4	588.2	109.2	170.9	317.1	102.3	167.7	288.8	69.6	128.7	281.6
768-77-1, 48	1081.08	402.1	569.2	908.9	176.8	262.4	432.4	115.8	173.7	299.3	60.1	119.4	251.8
768-78-1, 27	1085.87	268.8	400.9	725.6	135.5	211.9	392.1	113.2	191.1	352.8	77.6	148.1	348.5
768-79-1, 38	1090.98	568.6	691.2	1092.3	227.6	304.6	477.1	118.4	193.8	355.2	79.2	138.6	282.0
768-80-1, 77	1096.37	306.6	465.9	790.2	154.8	245.2	438.2	136.7	228.1	415.1	98.5	184.4	460.2
768-81-1, 19	1100.79	281.4	389.7	770.4	143.6	226.8	380.6	137.8	233.8	421.8	94.4	175.7	506.6
768-82-2, 17	1107.22	368.0	568.9	865.4	181.1	234.3	469.1	112.0	195.2	369.2	74.2	141.4	334.8
768-83-1, 137	1111.97	797.9	1073.6	1468.6	323.0	490.5	832.1	159.2	258.4	423.3	97.1	160.4	326.5
768-84-2, 93	1118.03	211.5	311.4	623.1	110.5	185.5	367.6	107.6	188.6	369.5	80.8	160.3	444.6
768-88-1, 28	1146.28	132.4	204.0	384.1	76.0	124.0	247.5	75.9	131.9	250.9	61.3	117.6	281.4
768-88-2, 114	1148.46	97.0	136.2	261.5	44.9	69.6	123.5	42.8	66.4	107.6	26.9	46.7	87.0
768-89-1, 77	1156.47	87.6	113.0	191.3	35.4	48.4	86.8	29.3	41.8	60.3	15.2	25.1	38.5
768-89-2, 5	1157.25	36.7	50.9	97.7	17.6	26.6	45.7	16.5	24.8	38.5	11.3	18.3	31.0
768-89-4, 50	1160.12	49.3	68.4	127.3	21.9	31.8	59.6	16.6	24.8	39.6	11.8	18.3	31.4
768-90-2, 59	1167.2	75.1	93.7	169.9	30.6	43.9	80.8	27.5	39.2	60.8	15.6	26.1	44.5
768-90-3, 50	1168.41	48.9	69.5	123.8	20.3	30.1	56.7	16.0	24.4	40.9	10.5	17.2	30.4
768-90-5, 72	1171.49	44.4	63.9	116.3	18.0	27.1	52.3	15.9	23.8	38.9	10.3	17.4	32.7
768-90-7, 104	1174.12	36.1	49.0	120.7	16.4	24.1	44.7	14.1	21.9	34.1	9.8	16.1	28.4
768-91-1, 32	1175.22	41.1	54.3	87.5	17.6	25.5	48.9	14.7	21.5	34.6	9.8	16.0	27.1
768-92-2, 22	1186.17	80.6	116.4	187.4	31.2	44.5	78.6	17.3	27.7	45.2	10.7	18.0	31.5
768-92-3, 135	1188.55	43.2	53.9	105.9	16.6	24.2	46.4	13.0	20.2	33.7	8.3	14.1	26.1
768-93-2, 12	1193.12	122.2	164.6	271.5	47.3	73.5	125.4	24.9	40.5	71.3	16.0	29.2	56.5
768-95-1, 4	1210.44	478.1	639.1	1010.6	209.6	280.4	490.3	107.8	165.2	278.5	62.0	113.2	222.0
768-96-1, 106	1221.06	291.2	378.6	587.0	119.9	156.0	237.6	70.7	101.5	139.4	29.8	51.3	82.5
768-97-3, 65	1233.11	165.3	225.2	339.1	68.8	97.2	130.9	31.1	48.3	68.5	15.5	25.0	39.6
768-98-1, 48	1239.88	204.5	269.4	430.2	87.3	120.5	196.0	85.6	123.9	173.6	43.0	75.9	119.8
768-98-2, 54	1241.44	73.5	88.4	138.4	21.5	28.3	55.4	28.3	40.4	50.0	14.4	23.3	33.4
768-99-3, 98	1252.92	195.5	252.8	421.9	80.3	115.2	203.8	72.5	110.7	168.4	36.8	65.1	117.0
768-100-1, 36	1259.16	157.9	225.8	435.9	78.0	124.5	238.5	83.2	137.4	249.9	50.6	102.5	212.3
770B-16-4, 26	421.41	18.8	24.0	41.8	5.8	9.7	15.0	3.0	4.6	7.2	1.7	2.8	5.0
770-2-2, 80	425.47	24.7	41.1	52.8	10.4	15.5	31.7	9.4	14.1	23.6	6.8	11.0	19.4
770-3-2, 72	435.12	20.9	42.8	65.7	10.8	16.8	35.8	10.3	15.2	26.0	7.9	12.7	22.7
770-3-3, 23	436.13	47.5	66.9	131.6	24.1	37.8	73.7	23.8	36.9	64.9	18.0	30.4	55.6
770-3-4, 102	438.42	29.1	49.9	89.9	15.4	23.8	47.6	14.2	22.5	39.2	11.5	18.7	33.3
770-4-1, 29	442.89	27.0	42.3	42.1	9.2	12.7	22.9	3.2	4.4	7.1	1.8	2.6	4.5
770-5-1, 67	452.87	13.7	27.5	42.6	5.2	8.1	17.4	3.2	4.7	9.4	2.3	3.6	6.9
770-5-3, 40	454.96	15.7	21.3	45.9	6.3	9.7	20.7	4.2	6.6	12.5	3.0	5.0	9.8
770-5-4, 37	456.19	27.3	36.1	68.8	10.0	14.3	28.5	6.5	9.3	16.1	4.2	6.3	11.2
770-5-7, 27	460.21	17.3	26.6	61.2	7.2	11.5	24.0	4.6	7.7	14.2	3.6	6.0	11.5
770-6-1, 82	462.72	21.4	30.6	56.3	9.2	15.1	31.3	8.0	13.6	23.9	6.1	10.7	20.8
770-6-3, 116	465.9	70.8	99.8	121.2	25.1	29.6	55.4	8.0	14.4	22.5	4.8	8.0	13.1
770-6-5, 107	468.81	21.5	31.0	73.5	9.5	14.9	29.3	7.5	11.3	20.5	5.4	8.7	16.7
770-7-1, 27	471.77	35.7	53.1	78.5	14.5	21.3	43.4	13.3	19.6	31.7	8.4	14.0	24.5
770-7-3, 84	475.17	28.4	60.0	70.5	12.2	18.9	37.2	10.1	15.6	26.3	6.9	11.9	23.2
770-7-5, 107	478.21	19.6	28.4	56.0	8.8	15.6	27.4	7.1	10.7	18.2	5.4	8.4	14.6
770-9-2, 120	493.5	21.1	34.1	65.2	10.3	16.8	34.2	9.0	14.4	26.4	7.3	12.1	23.3
770-9-2, 29	492.59	38.7	58.1	103.1	19.0	29.7	58.3	17.3	27.0	45.9	13.0	21.8	38.3
770-10-1, 140	501.9	30.8	47.5	98.2	14.3	21.8	42.3	11.4	17.9	31.1	8.8		
770-10-2, 9	502.09	25.5	37.3	74.3	11.5	18.2	35.3	10.3	15.7	27.6	7.9	12.8	22.6
770-10-3, 8	503.47	41.0	57.6	105.4	17.3	25.0	46.6	16.0	21.5	33.3	10.1	16.1	27.1
770-11-2, 99	512.52	40.9	61.7	101.7	17.2	25.5	47.3	12.3	20.4	34.7	8.8	15.0	27.9
770-12-1, 8	519.98	24.6	33.5	68.8	10.9	17.2	33.9	7.7	12.6	23.9	6.0	10.0	19.4
770-12-2, 66	522.06	54.8	68.5	123.4	18.5	26.7	47.5	9.0	12.9	20.9	5.0	8.0	14.1
	C_w (S/m):	8.31	11.43	17.32	3.16	4.53	7.28	0.54	0.79	1.35	0.16	0.23	0.39

spheric pressure. Bridge accuracy was repeatedly checked with a 20-kΩ resistor, yielding <1% variance of replicate measurements. Samples were first wrapped in teflon tape, except for cylinder ends. Silver-screen electrodes were clamped to the cylinder ends, with intervening thick saturated filter paper. The resistance contribution from the wire, electrodes, and filter paper was measured at each salinity and temperature, using a copper standard replacing the sample. These system resistances were subtracted from all sample measurements. More than 90% of the system resistance was attributable to the wet filter paper, but the filter-paper benefits of assured electrode and sample endpiece saturation and of improved replicability were deemed to outweigh the larger system resistance, particularly since the system resistance was so low that it was negligible for almost all measurements. Conductivities shown in Table 2 and discussed subsequently are corrected by subtracting the following system resistances: 123Ω for 1.2 ppt, 36Ω for 4.4 ppt, 6.3Ω for 29.5 ppt, and 2.4Ω for 87.6 ppt.

Samples were saturated and measured at four salinities, in the following order: 29.5 ppt, 87.6 ppt, 4.4 ppt, and 1.2 ppt. At each salinity, samples were measured at three temperatures: 10°C, 25°C, and 50°C. Except during measurement, samples were kept immersed in an actively circulating temperature bath with confirmed accuracy of 0.02°C. However, temperature drift of as much as 0.08°C was tolerated at the 50°C measurement level, because this drift is trivial compared to the cooling of perhaps 1-3°C that probably occurred during the 30 seconds required to clamp and measure each sample. To minimize this measurement time, particularly for occasional

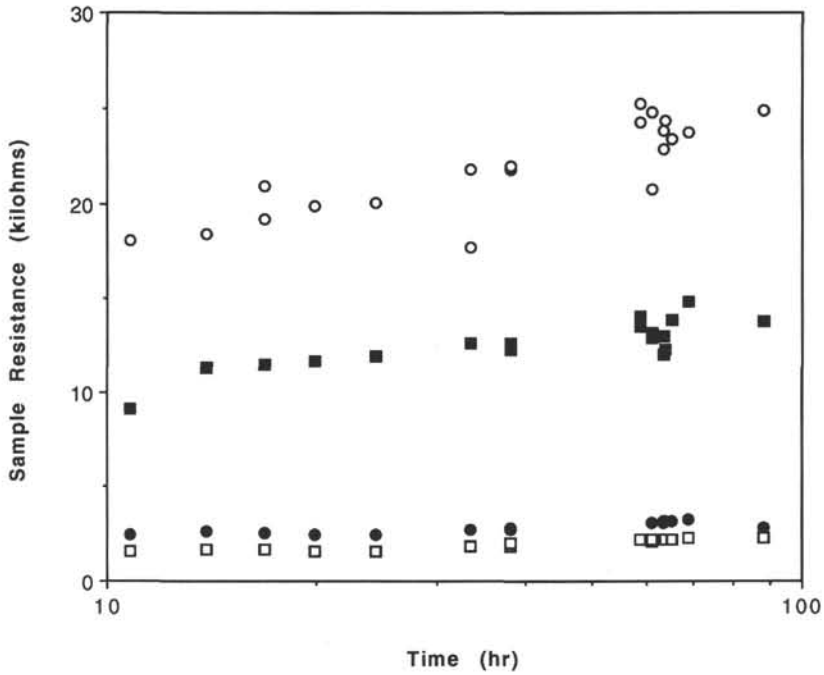

Figure 3. The change in resistivity as a function of time for four test samples, as the internal salinity of the samples gradually equilibrates to the change in surrounding fluid from 87.6- to 4.4-ppt salinity. Resistance increases with the logarithm of time, as expected for a diffusion process. Based on this plot, about 60–90 hr were judged to be the minimum permissible time for sample equilibration to a new salinity.

samples that were subject to drift with longer measurement times at high temperature, two experimenters were needed. The fluid temperature limits of 10°–50°C were judged to be the tolerable temperature extremes for prolonged exposure of a human arm.

Except for the initial 29.5 ppt saturation by vacuum impregnation, changes in sample salinity were achieved by changing the salinity of the temperature bath, continuing vigorous fluid circulation, and waiting for sample equilibration with the new salinity. The times permitted for equilibration before the start of measurements at each salinity were 35 days for 29.5 ppt, 7.8 days for 87.6 ppt, 68.6 hours for 4.4 ppt, and 61.1 hours for 1.2 ppt. For equilibration at the latter two salinities, resistivity of four samples was measured as a function of time (Fig. 3) to determine the minimum required equilibration time. In view of the earlier difficulty in accessing some pores during drying, even these very long equilibration times do not assure that all samples have achieved complete salinity equilibration with the surrounding fluid.

At each temperature and salinity, about 10% of the samples were measured more than once, in order to determine replicability of measurements. As shown in Figure 4, replicability was better than 5% for most tests, throughout the range of resistivities measured. Replicability was slightly worse for 50°C measurements than for those at 10°C and 25°C (Fig. 4), possibly due to greater temperature change and drying of the samples during measurement.

Measurements of cation exchange capacity (CEC) were made on 46 samples selected from the two sites. The measurement of CEC (Ridge, 1983) is widely used in the oil industry to indicate the potential of shale effects on log responses of a sedimentary formation. This electrochemical analysis is utilized to count the number of free cations that might contribute to the conduction of current during electrical measurements. Clay minerals such as smectites and to a lesser extent chlorites are often observed as alteration products of oceanic basalt phases (Alt and Emmermann, 1985; Alt et al., 1986; Adamson, 1979, 1985) and are characterized by large CEC values (Serra, 1984; Ellis, 1987). The Jackson Modified CEC Method (Fig. 5), a standard technique to determine the CEC of rocks (Ridge, 1983; Pezard, 1990), was applied to the samples.

Each of the 46 samples was cleaned, dried, and crushed to a grain size >74 mm. Quantities of 1–2 g were selected after a thorough mixing to assure maximum homogeneity. The clays were dispersed with distilled water, then carbonates were removed by washing the sample three times with buffered acetic acid. Equilibration of the sample with ammonium ions was achieved by three washing cycles with ammonium acetate (Fig. 5). A final two washings of the sample with reagent alcohol was utilized to prevent the clays from hydrolyzing.

In a Kemmerer Distillation Unit, sodium hydroxide was used to displace the ammonium ions from the possible cation exchange sites; displaced ammonium ions were collected as ammonia. The NH_4 content was determined via titration with hydrochloric acid. The CEC value is then obtained by:

$$[(\ ml\ HCl\ ) \cdot (\ meq\ HCl/ml)/sampleweight] \cdot 100 = meq/100\ g \quad (1)$$

Laboratory tests on standards indicate that this technique has a precision of 0.1 meq/100 g and a sensitivity of 0.5 meq/100 g. However, the procedure is somewhat operator-dependent, and interlaboratory replicability is much lower. In particular, excessive grinding of the sample can seriously degrade replicability.

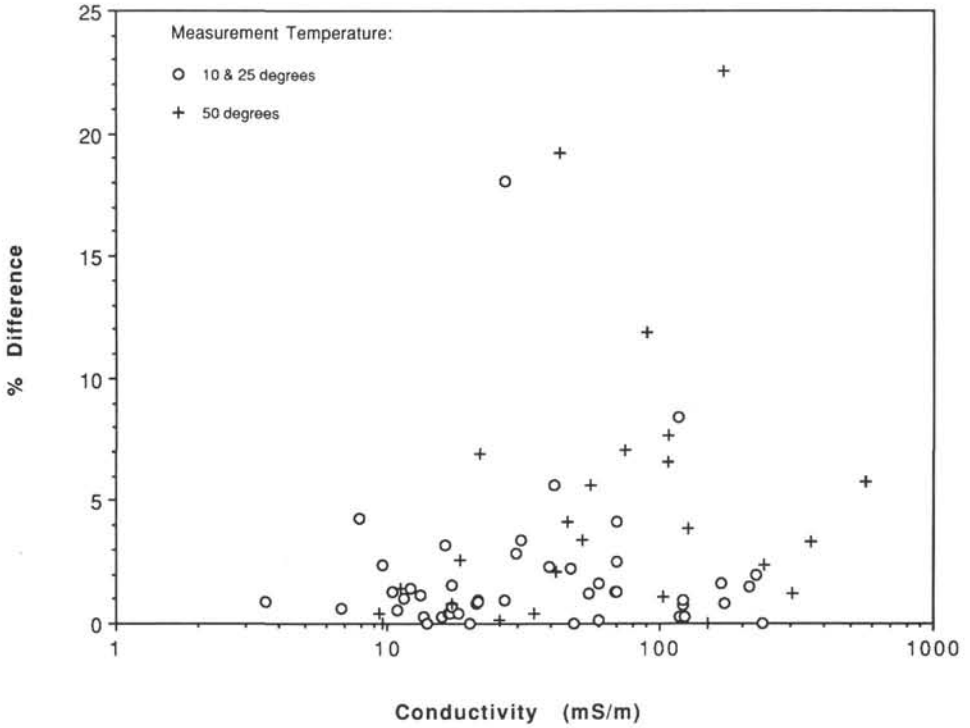

Figure 4. Percentage difference between replicate conductivity measurements as a function of sample conductivity. Throughout the range of observed sample conductivities, replicability was normally better than 5%. Measurements at 50°C exhibited slightly greater dispersion than those at lower temperatures.

MODELS

Resistivity (and its inverse, electrical conductivity) of rocks is primarily dependent on porosity and the resistivity of pore fluids. In crystalline rocks, the topology of the pore space (e.g., crack geometry) may be as important as total porosity in determining sample resistivity, and clays also can have substantial influence on resistivity. According to the Archie (1942) empirical equation as generalized by Winsauer and McCardell (1953),

$$FF = a \cdot \phi^{-m} \quad (2)$$

where FF, the formation factor, is equal to the ratio of formation resistivity (R_o) to formation water resistivity (R_w), ϕ is fractional porosity (not percentage porosity as in Table 1 and the figures), and both a and m are constants. In the petroleum industry, m is termed the cementation factor, but m probably has no relation to cementation in crystalline rocks. Here we express FF in terms of the total measured conductivity of the rock (C_o) and the conductivity of pore fluid (C_w): $FF = C_w/C_o$. Both a and m must be locally determined from relations among the other variables, and the other variables can be determined either by analysis of core samples or *in-situ* logs. Typical empirical values for a and m are 0.8 and 2 for carbonates and 1 and 1.8 for sandstones. However, the very different pore geometry of basalts generally leads to estimates of about 4–30 for a and 0.9–1.8 for m, as summarized by Pezard (1990).

The Archie equation is only appropriate for "clean" formations with no clay, as it requires that sample conductivity be entirely attributable to the conductivity of the fluids within an infinitely resistive solid. A second type of conductivity is surface conduction on clays. The conductivity per unit volume is an order of magnitude higher for seawater than for clay at room temperature. Nevertheless, clay surface conductivity dominates pore conductivity in low-porosity shales; it may also play an important role in some altered basalts, where it can cause resistivity-derived predictions of porosity to be too high. For example, at Hole 504B a large interval of low resistivity was initially interpreted as having moderate porosity (Becker, 1985) and yet had low permeability (Anderson, et al., 1985; Becker, 1989). This apparent paradox was resolved by hypothesizing that conductive clay alteration products have sealed cracks and lowered permeability (Pezard and Anderson, 1989).

The temperature dependence of surface conduction appears to be higher than the temperature dependence of pore-fluid conduction, due to higher activation energy; thus Olhoeft (1981) concluded that surface conduction can be negligible at room temperature and yet be dominant over pore conduction at temperatures above 80°C. This difference in temperature response of the two conductive components is the motivation for our choice of an experimental design that includes both temperature and salinity as independent variables. Both temperature and salinity affect pore fluid conductivity, whereas only temperature substantially affects clay surface conductivity.

For crystalline rocks such as basalt, sample conductivity exhibits a relationship to fluid conductivity that may be describable by the idealized model of Figure 6. For two resistors in parallel, conductances are additive. At high fluid conductivity, the dominant conductivity component is proportional to fluid conductivity; this component is clearly pore fluids. At low fluid conductivity, rock conductivity in the idealized model is independent of fluid conductivity; this component is normally assumed to be surface-layer conduc-

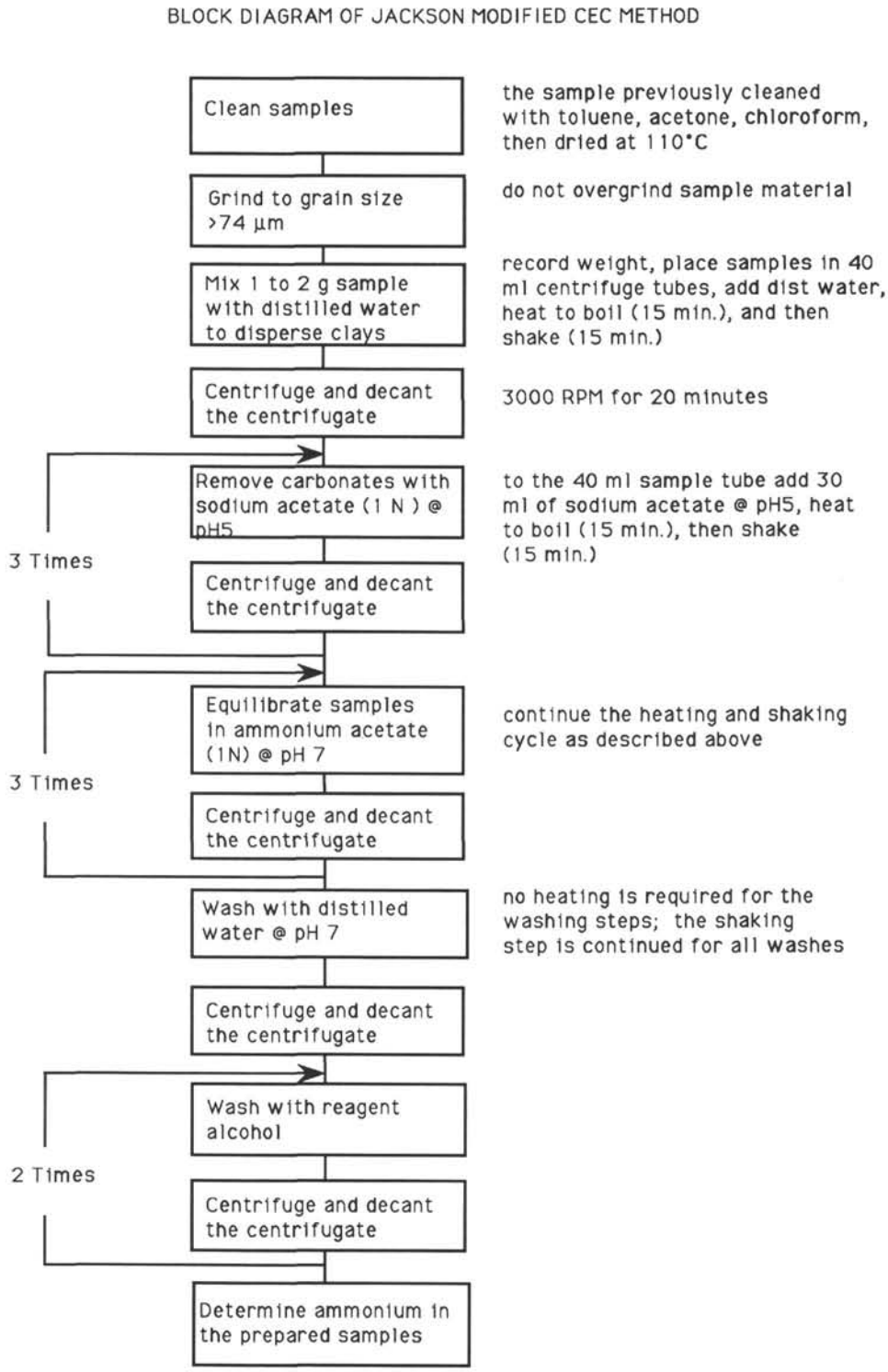

Figure 5. Block diagram of the Jackson Modified CEC Method.

tion on clays (Pape et al., 1985; Flovenz et al., 1985; Pezard, 1990). Note that with the log/log scaling, each component quickly becomes negligible as one moves into the realm in which the other component is dominant. However, the range of salinities used in our (and most other's) laboratory measurements does not achieve complete flattening of the curve to a constant, C_w-independent value. Similarly, the possibility of residual clay effect even at high salinities (Fig. 6) must be investigated.

Pape et al. (1985) and Pezard (1990) considered the total conductivity when both fluids in open pores and surface conduction of clays are present:

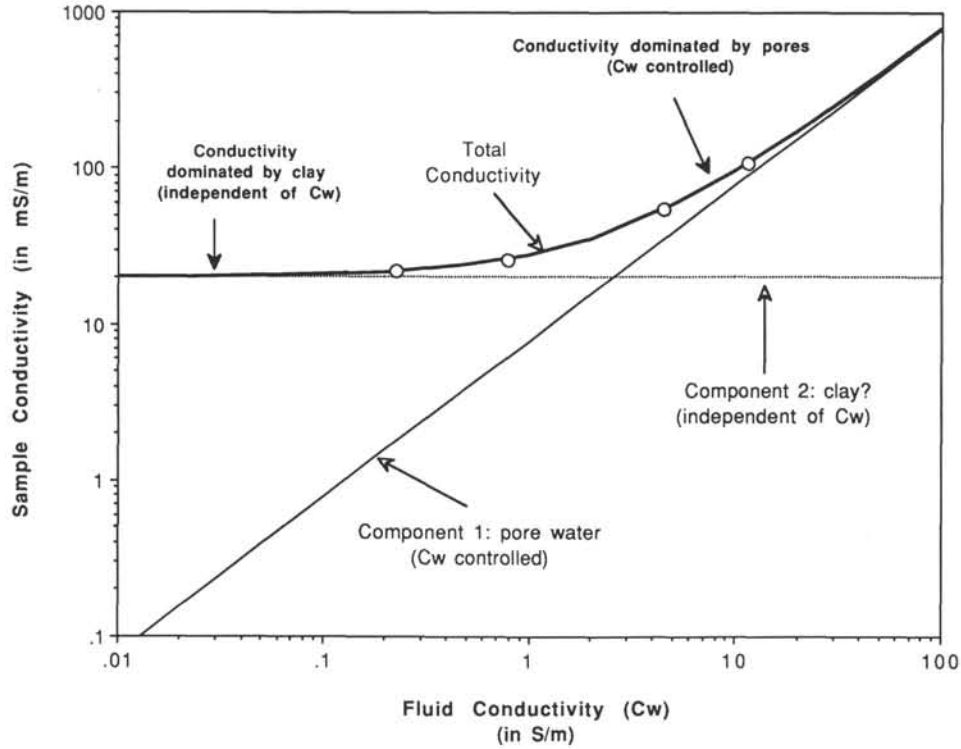

Figure 6. Idealized diagram of the relationship of sample conductivity to fluid conductivity for a basalt similar to those of the present study and with a porosity of 10%. Our conductivity measurements (e.g., Fig. 7; Table 2) for any one temperature exhibit a curved pattern similar to the bold line; open circles show the positions of points measured at 25°C.

$$C_o = C_w/FF + B \cdot CEC \cdot \rho\beta \cdot (1-\varnothing)/(\varnothing \cdot \mu^2 \cdot FF) \qquad (3)$$

where FF is the "intrinsic" formation factor (determined at high salinity where clay contribution is negligible and therefore $FF = C_w/C_o$), B is the sodium charge mobility, CEC is the cation exchange capacity per 100 g of rock, ρb is the bulk density, ϕ is the fractional porosity, and μ^2 is a tortuosity factor associated with the topology of pore surfaces. Although this tortuosity factor is probably variable and its value is unknown in our study, several authors (Pape et al., 1985; Wilkens et al., 1989; Pezard, 1990) have assumed a value of 10 for $\mu 2$. We shall do the same for testing purposes, but the subsequent tests investigate correlations that are independent of the actual value of $\mu 2$.

A nonlinear pattern such as in Figure 6 is routinely observed in both shales and basalts, and the pattern is routinely interpreted to be associated with the two components, pore fluid and clay surface conduction. Often linear rather than logarithmic scaling is utilized, and a linear fit to the data for a shaly sample gives a finite rock conductivity at zero fluid conductivity, implying the presence of a C_w-independent component (Waxman and Smits, 1968). This C_w-independent component appears to be clay surface-layer conductivity for shales, but for basalts an alternative explanation warrants consideration.

The C_w-independent portion of the curve could be due not to clays but instead to microcracks, which can create a C_w-independent component either because of non-clay surface-layer conduction or because the microcracks have too little permeability for laboratory displacement of their fluids by new fluids of controlled C_w. We have already demonstrated that some cracks have so little permeability that reliable porosities and grain densities cannot be obtained without prolonged drying at very high vacuums. We therefore hypothesize that these cracks, and even less-permeable cracks, would have a conductivity controlled by their own initial salinity (seawater), independent of any reasonable amount of circulating fluids of differing salinity and C_w.

A thin clay-lined crack may be permeable at high salinity, yet impermeable at low salinity due to increased thickness of the Helmholtz layer (Matijevic, 1974). Gradual clay filling of a variable-width crack will cease when the narrowest portion shrinks to twice the thickness of the Helmholtz layer. The majority of the crack still contains seawater, which is impermeable to convective flow, difficult to drive off by drying, and capable of salinity change only by the very slow mechanism of osmotic flux through a high-aspect-ratio path. A human analogy is clogged arteries.

The two hypotheses lead to different predictions concerning the value of C_o at low fluid conductivity. The clay-conduction model predicts a strong positive correlation of observed C_o with clay content, expressed as CEC, at low fluid conductivity (equation 1). In contrast, a microcrack model, with either impermeable cracks or non-clay surface-layer conductivity, predicts no direct relationship of CEC to C_o at low fluid conductivity, although an indirect correlation is possible if greater porosity permits greater alteration. The microcrack model does predict a strong correlation between C_o and porosity at low fluid conductivity, because greater porosity implies more cracks of all sizes. In contrast, the clay-conduction model of equation 1 predicts that the contribution of porosity to C_o is very small at low fluid conductivity.

The two hypotheses may also lead to different predictions concerning the temperature dependence of C_o at constant

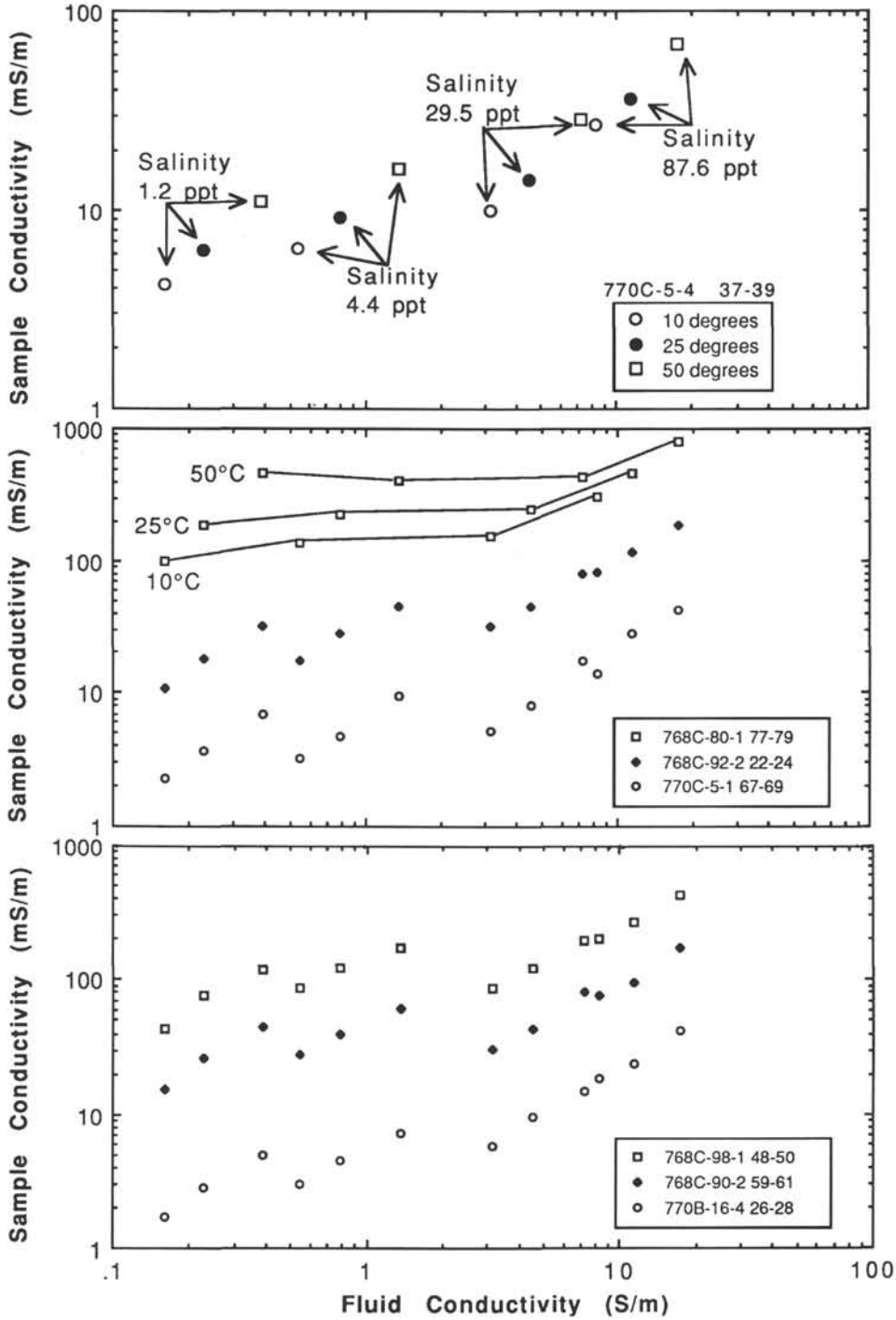

Figure 7. Seven examples (of the 54 in Table 2) of sample conductivity as a function of fluid conductivity. Each sample was measured at three temperatures for each of four salinities, permitting examination of the effect of both variables on sample conductivity. Both variables also affect fluid conductivity, as shown in the top example. Leg 124 sample numbers are given.

salinity, if the activation energy of clay conduction is higher than that of pore conduction.

DISCUSSION

Figure 7 shows seven examples of C_o vs. C_w crossplots obtained in this study; similar data for all 54 samples are tabulated in Table 2. Within each of the three temperatures used, the trend of points at the four salinities is generally similar to the idealized model of Figure 6, except for less flattening at low C_o than in Figure 6. Increasing temperature shifts the entire curve upward and somewhat to the right. This shift is exactly the pattern expected for clay conduction,

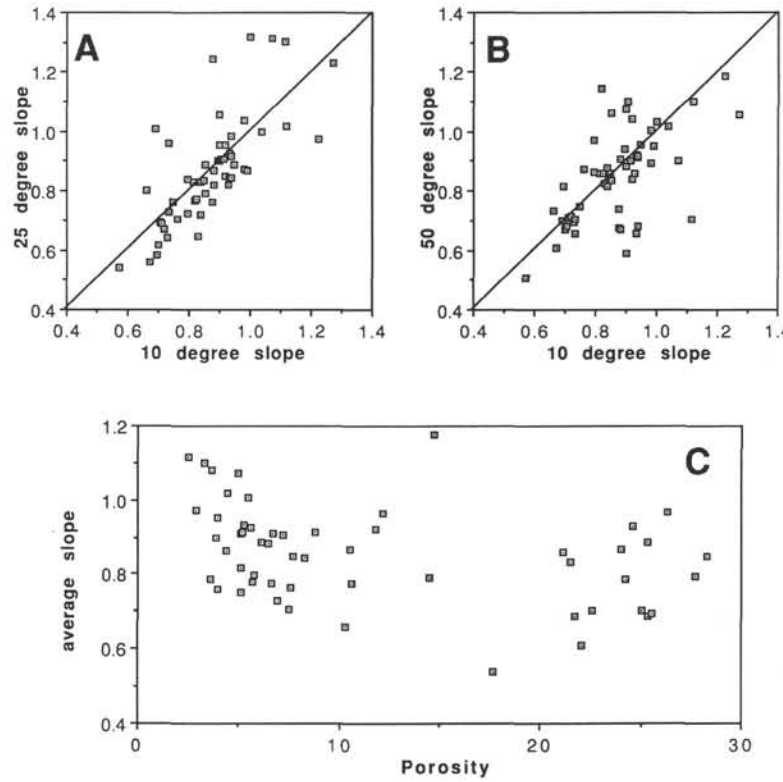

Figure 8. Slope of the variation of sample conductivity as a function of fluid conductivity at high salinity for each of the three temperatures 10°C, 25°C, and 50°C (**A**) and (**B**). Although dispersion is substantial, no systematic decrease in slope is noted for increasing temperature, as expected for a clay contribution to sample conductivity. Ratios are, however, consistently less than one, indicating that some component independent of fluid conductivity is present (e.g., Fig. 6). Slope does not depend on sample porosity (**C**).

which is highly temperature dependent. Unfortunately, it is also the pattern expected for impermeable crack conductivity and is therefore not immediately diagnostic.

Formation Factor

One of the objectives of this study is determination of the relationship of the intrinsic formation factor $FF = C_w/C_o$ to porosity, yielding the Archie coefficients a and m. Although data such as Figure 7 do not conclusively demonstrate that the low-salinity C_w-independent component of equation 1 and Figure 6 is present, caution is required to assure that our estimate of FF is not affected by such a component. We have determined the intrinsic formation factor of each sample in two ways. First, one can simply determine $FF = C_w/C_o$ at a C_w high enough to be on the linear portion of the C_w vs. C_o curve of Figure 6. Second, one can use regression to solve equation 1 for the C_w-dependent and C_w-independent components.

At high fluid conductivities where pore-fluid conduction is dominant, one might expect that all points for a given sample would fall on the same C_o/C_w line. In other words, rock conductivity would depend only on fluid conductivity, regardless of the combination of salinity and temperature used to obtain each fluid conductivity. To a first approximation, such a pattern is observed, in Figure 7 as well as in nearly all other samples.

If Olhoeft's (1981) generalization is correct that clay conduction becomes dominant above 80°C in oceanic basalts, the two high-salinity (high-C_w) 50°C points should lie above the C_o/C_w line formed by the four 10° and 25°C points. Such a pattern is not observed in our data; possible explanations include absence of significant clay conduction, similar temperature dependencies of activation energy for clay and seawater, or different electrical properties in our clay minerals than in those studied by Olhoeft (1981).

In Figure 7 and many other samples of Table 2, one sees a pattern of variable, sample-dependent vertical (or horizontal) offset of the three points obtained at 29.5 ppt salinity with respect to the group of three points at 87.6 ppt salinity. One possible explanation of this offset is incomplete replacement of the pore fluid by fluid of the new salinity, as suggested by the impermeable-crack model. If so, it should be noted that the 8–35 days allowed for pore-fluid equilibration at these two salinities is already much longer than the times allowed in most other studies. However, reliable interpretation of this offset must await repeat saturations at the two salinities. For this reason, several samples were withheld from crushing for CEC measurements.

For each sample, the slope of our two highest-salinity points (29.5 and 87.6 ppt) might be expected to decrease with increasing temperature, because temperature-induced increase in C_w-independent component would shift the entire C_w/C_o curve upward and to the right. However, comparison of slopes obtained at different temperatures fails to detect this effect: Figure 8 shows that the 25°C slopes tend to be slightly higher than 10°C slopes, and 50°C slopes are generally similar to 10°C slopes. Pezard (1990) has noted that the C_w-indepen-

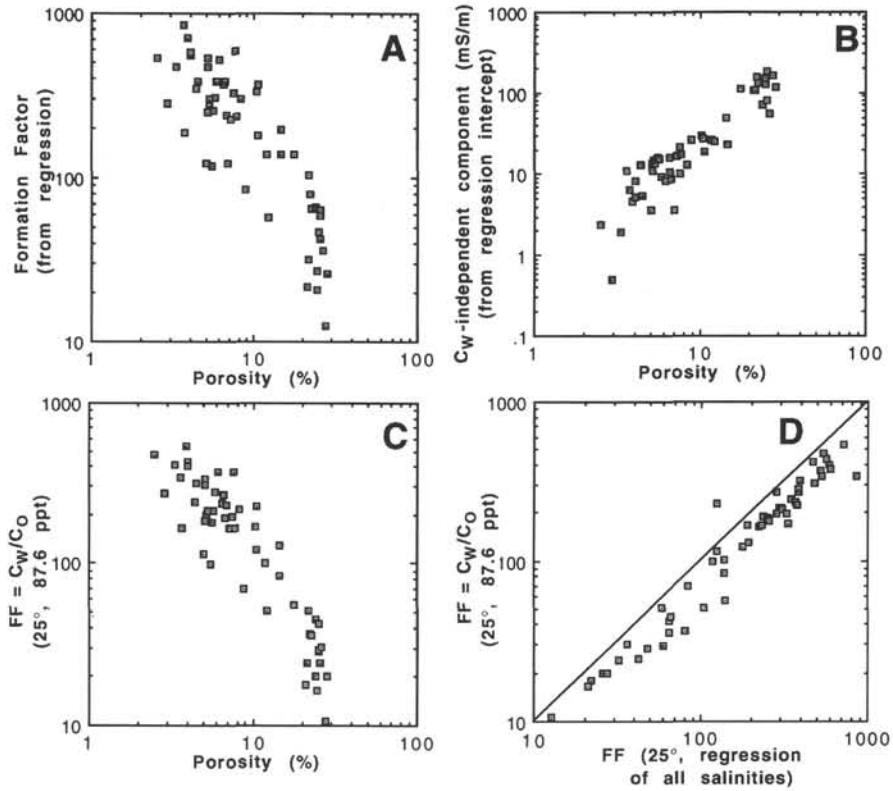

Figure 9. The two components illustrated in Figure 5, one related to formation factor and one independent of fluid conductivity, were determined by regression of sample conductivity on fluid conductivity for 25°C measurements, then plotted as a function of porosity in (**A**) and (**B**), respectively. In (**C**), formation factor was calculated from the ratio of fluid to sample conductivity for the measurement at 25°C and 87.6-ppt salinity, then plotted as a function of porosity. Both techniques of estimating formation factor yield roughly similar values and similar relations to porosity, but the regression values are about 20% higher than the single-measurement values (**D**). The component independent of fluid conductivity is nevertheless very highly dependent on sample porosity (**B**).

dent component extends to higher C_w for high-porosity pillow basalts than for more massive flows; he attributes this pattern to greater alteration in the pillows. Comparison of average slope at high C_w to porosity (Fig. 8) shows that this pattern is present but is weak; slope is almost independent of porosity.

Do our high-salinity measurements indicate formation factor, without any contamination from C_w-independent components? If both of the high-salinity points (29.5 and 87.6 ppt) for each temperature are entirely controlled by pore fluids with negligible contribution from a C_w-independent component, then we expect the slope of these two points to equal one on a logarithmic plot of C_o vs. C_w (e.g. Figs. 6 and 7), for each sample at each of the three temperatures. Figure 8 shows that the slopes are consistently less than one for all temperatures, indicating that at least some C_w-independent component is present in the 29.5-ppt assemblage. This test does not allow us to evaluate whether or not the 87.6-ppt measurements also include a significant C_w-independent component.

A second approach should enable us to determine intrinsic formation factor even in the presence of a pervasive C_w-independent component. Equation 1 is of the form $C_o = k_1 \cdot Cw + k_2$, where $k_1 = 1/FF$ and $k_2 = B \cdot CEC\rho_b(1-\phi)/(\phi \cdot \mu\perp^2 \cdot FF)$. For measurements of C_o as a function of C_w at constant temperature, both k_1 and k_2 are expected to be constant for each sample, not between samples. Thus we can determine k_1 and k_2 for each sample by regression of the four $[C_w, C_o]$ pairs. We chose to do so for T = 25°C measurements. Note that k_2 can be interpreted as due to clay conduction as implied by equation 1 and the k_2 definition above; however, this approach is not dependent on the assumption that the C_w-independent component is clay conduction. This approach assumes only that two conductors are in parallel, with one dependent on fluid conductivity.

Nearly all of the 54 regressions account for more than 90% of the variance of C_o, and most account for more than 95%. However, in plotting the 54 regressions we noted a very consistent pattern of deviations of observed C_o from the regression line: the 4.4- and 87.6-ppt points fall above the line, while the 1.2- and 29.5-ppt points fall below the line. The regression assumption of random errors is therefore violated, and the fitted slopes must be treated with some caution.

Formation factor determined by regression is consistently about 20% higher than *FF* calculated simply from the ratio C_w/C_o at 25°C and 87.6 ppt (Fig. 9). This difference could imply that the latter technique is underestimating *FF* because of a small C_w-independent component even at our highest salinity. The regression estimates of residual (intercept) C_o when C_w approaches zero are consistently several percent of the C_o for high salinity, suggesting that even our highest salinity does contain a trace of C_w-independent component. The 20% difference between the two techniques is minor in comparison to the order of magnitude range of observed formation factors (Fig. 9).

Table 3. Estimation of Archie coefficients a and m, by regression of sample conductivity (C_o) on porosity (ϕ) according to the relation $C_o = C_w \cdot \phi^m/a$. Note that only the regressions for 29.5 and 87.6 ppt are considered to yield reliable estimates of a and m, because of the presence of a component independent of fluid conductivity (C_w) at lower salinities (see text).

T (°C)	Salinity (ppt)	a	m	Corr. Coef.	Number of Points
10	87.6	4.60	1.36	0.906	54
25	87.6	4.78	1.33	0.910	52
50	87.6	4.37	1.31	0.922	52
10	29.5	3.39	1.44	0.926	54
25	29.5	3.40	1.42	0.928	54
50	29.5	3.32	1.37	0.934	54
10	4.4	0.63	1.53	0.967	54
25	4.4	0.55	1.56	0.964	54
50	4.4	0.58	1.55	0.954	54
10	1.2	0.33	1.46	0.951	54
25	1.2	0.23	1.55	0.953	54
50	1.2	0.17	1.63	0.936	54

Formation Factor vs. Porosity

For every batch of measurements at the same temperature and salinity, we used linear regression to determine the relationship of the ratio C_w/C_o to porosity (Table 3). At high C_w, the relationship of the intrinsic formation factor $FF = C_w/C_o$ to porosity yields the Archie coefficients a and m. At lower C_w, fluid conductivity is too low to dominate sample conductivity, so the ratio C_w/C_o does not equal formation factor. All relationships are very well determined, with correlation coefficients of 0.91–0.97, and all are based on more than an order of magnitude range of porosities. Site 770 porosities are generally lower than Site 768 porosities, but at each C_w data from the two sites appear to lie along the same trend of conductivity vs. porosity.

In the previous section we concluded that our highest salinity of 87.6 ppt is the most likely to yield reliable estimates of formation factor, with minimum effect from any C_w-dependent component. Figure 9 shows the relationship between C_w/C_o and porosity for 25°C and 87.6 ppt. Table 3 shows that virtually identical relationships of C_w/C_o to porosity are also obtained at 10°C and 50°C. Similarly, the three solutions for C_w/C_o vs. porosity for 29.5 ppt are statistically indistinguishable from each other. Presumably because of a minor C_w-independent component at 29.5 ppt, the 29.5-ppt estimates of the regression coefficients a and m are slightly different from the 87.6-ppt values (Table 3). This difference in coefficients is trivial in comparison to the range of other investigators' estimates of a and m in basalts (e.g., compilation by Pezard, 1990). Nevertheless, the more reliable 87.6-ppt coefficients do yield a predicted C_o that is up to 15% higher or lower, depending on porosity, than would be estimated with the 29.5-ppt coefficients.

The similarity of estimates for a and m (Table 3) for a wide range of salinity (29–88 ppt) and temperature (10°–50°C) has an important implication: one can use these coefficients to transform between C_o and porosity with logs, ignoring clay conductivity effects unless the logged section has much higher clay content than our core samples have. Based on the 88-ppt estimates of Table 3, $m \approx 1.3$ and $1/a \approx 0.22$, so the appropriate Archie relation is $C_o = 0.22 \cdot C_w \cdot \phi^{1.3}$.

Our estimate of m, like those of previous investigators who have estimated a and m for other basalts, is not much larger than unity, indicating that either high-aspect ratio pores or surface conduction is present.

Our estimates of a and m are within the range of those determined in other studies but significantly different from most. We do not attribute the differences to between-site variations, as we found very consistent patterns between Sites 768 and 770, although basalts at the two sites differ substantially in porosity and alteration. Certainly differences in analytical techniques are partially responsible, particularly for log-based vs. core-based studies. Additional sources of differences between studies are the narrow range of porosities in some studies and the failure to remove C_w-independent components and thereby determine intrinsic formation factor in others. Thus it is difficult to determine which apparent intersite variations in a and m are real.

For every batch of measurements at the same fluid conductivity, a strong correlation between sample conductivity and porosity is found (Table 3). This pattern is theoretically predicted only for high C_w, where $C_o = C_w \cdot \phi^{m/a}$. However, this pattern is consistently evident in Table 3, regardless of temperature or salinity. Of particular importance, this correlation is still present and indeed is strongest at the lowest two salinities, where both the clay conduction and microcrack mechanisms predict only a possible indirect correlation between Co and the dominant C_w-independent component. More porous samples could have easier and more pervasive alteration than less porous samples; they certainly have proportionately more area of cracks for potential surface conduction. However, neither pattern accounts for the observation of even better correlation at low C_w than at high C_w where pore conductivity is expected to cause a very strong correlation between sample conductivity and porosity.

Cation Exchange Capacity

The CEC data obtained for this study showed a high reproducibility (Table 4) as well as a high accuracy when standard clay samples were run. The CEC measurements exhibit only a weak correlation to porosity (Fig. 10A) and an even weaker correlation to predicted CEC values (Fig. 10B) based on regression estimation of the C_w-independent component. Thus the C_w-independent portion of electrical conduction does not appear to be related to the conduction of electrical currents via clay minerals. Instead, it appears to be strongly related somehow to porosity (Fig. 9B).

An alternative interpretation is that there is a slight clay (CEC) effect at high salinity and somewhat larger clay effect at low salinity, but not enough to destroy the good correlation between formation factor and porosity. However, the correlation between C_w/C_o and porosity is even higher at low salinity than at high salinity (Table 3), and Figure 10B implies an almost negligible CEC effect.

Clay Conduction or Microcracks?

We have noted the virtually identical relationships of the ratio C_w/C_o to porosity for different temperatures at the same salinity (Table 3), at least for the range of salinities 4.4–87.6 ppt. This pattern is difficult to reconcile with the combination of significant clay conduction and of a higher activation energy for clay conduction than for pore-fluid conduction. However, some systematic change with temperature of the relationship between C_w/C_o and porosity is apparent in the lowest salinity (1.2 ppt; Table 3), consistent with clay conduction. Alternatively, the microcrack hypothesis is consistent with our observation of temperature independence of C_w/C_o at 4.4–87.6 ppt but inconsistent with the temperature dependence at 1.2 ppt.

Of our several tests of clay conduction vs. either non-clay surface conduction on cracks or impermeable cracks as a

Table 4. Measurement of cation exchange capacity (CEC) for basalts from Leg 124 Sites 768 and 770.

Sample Loc.	mbsf	CEC	CEC repeat
768-74-1, 115	1057.450	8.9	
768-74-2, 37	1058.120	17.1	16.9
768-77-1, 48	1081.080	11.3	11.5
768-78-1, 27	1085.870		
768-79-1, 38	1090.980	11.4	11.5
768-80-1, 77	1096.370	10.3	
768-81-1, 19	1100.790	14.6	14.0
768-82-2, 17	1107.220	11.7	11.5
768-83-1, 137	1111.970	10.6	10.6
768-84-2, 93	1118.030	9.8	9.4
768-88-1, 28	1146.280	9.6	
768-88-2, 114	1148.460	6.9	7.0
768-89-1, 77	1156.470	5.8	
768-89-2, 5	1157.250		
768-89-4, 50	1160.120		
768-90-2, 59	1167.200	8.9	9.2
768-90-3, 50	1168.410	6.1	6.1
768-90-5, 72	1171.490	5.9	6.0
768-90-7, 104	1174.120	5.1	
768-91-1, 32	1175.220	6.4	
768-92-2, 22	1186.170	4.8	4.9
768-92-3, 135	1188.550	5.2	
768-93-2–12	1193.120	5.9	6.2
768-95-1, 4	1210.440	9.7	
768-96-1, 106	1221.060	9.3	9.2
768-97-3, 65	1233.110	9.7	
768-98-1, 48	1239.880	9.2	
768-98-2, 54	1241.440		
768-99-3, 98	1252.920	9.9	
768-100-1, 36	1259.160		
770B-16-4, 26	421.410	3.1	
770-2-2, 80	425.470	13.8	
770-3-2, 72	435.120	14.4	
770-3-3, 23	436.130	23.4	
770-3-4, 102	438.420	19.2	19.0
770-4-1, 29	442.890	19.1	
770-5-1, 67	452.870	12.1	
770-5-3, 40	454.960		
770-5-4, 37	456.190		
770-5-7, 27	460.210	18.2	
770-6-1, 82	462.720	16.3	
770-6-3, 116	465.900	26.0	26.2
770-6-5, 107	468.810	3.2	3.3
770-7-1, 27	471.770	9.3	
770-7-3, 84	475.170	8.3	
770-7-5, 107	478.210	8.6	8.5
770-9-2, 120	493.500	5.7	
770-9-2, 29	492.590	8.2	8.7
770-10-1, 140	501.900	8.1	
770-10-2, 9	502.090	7.8	
770-10-3, 8	503.470	8.3	
770-11-2, 99	512.520	9.1	
770-12-1, 8	519.980		
770-12-2, 66	522.060	6.9	6.8

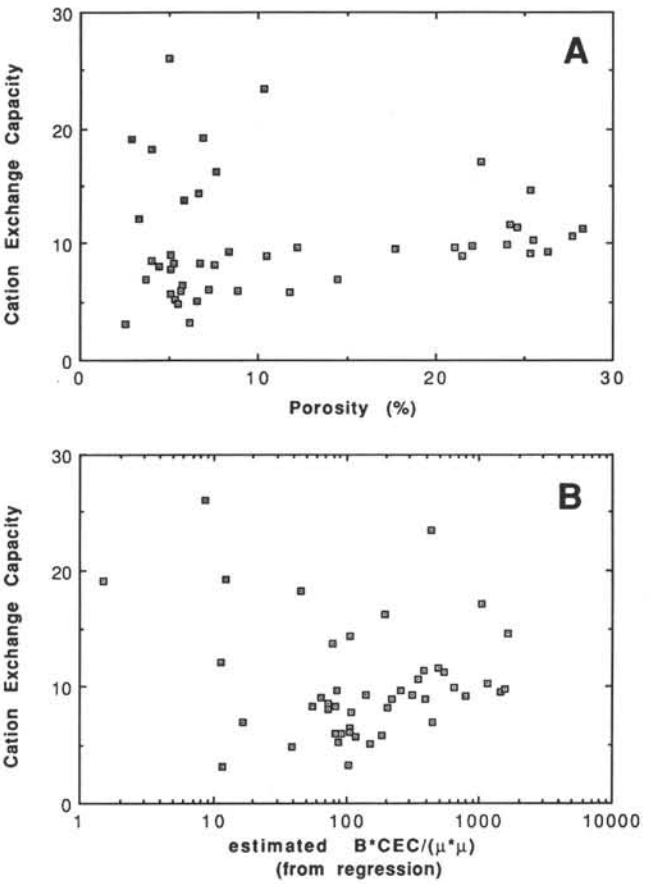

Figure 10. **A.** Relationship between cation exchange capacity and porosity of the 46 samples with determined CEC values). **B.** Comparison of experimentally determined CEC values with estimates of CEC values obtained via equation 1 and the regressions of Figure 9; the poor correlation is difficult to reconcile with the equation 1 model of a clay-conduction contribution to measured sample conductivity.

source of C_w-independent sample conductivity, none diagnostically establish one mechanism to the exclusion of the other. The concept of impermeable cracks depends of course on one's laboratory time scale: we have seen that sample conductivity continues to change in response to changed fluid conductivity for at least 100 hr (Fig. 3), and that shipboard drying times for porosity determination are inadequate (Fig. 1 and 2). Incomplete flushing of cracks by a new salinity despite 8 days for equilibration is just one possible interpretation of the offsets between 29.5- and 87.6-ppt conductivities on plots of C_o vs. C_w such as Figure 6. An impermeable-crack mechanism more successfully accounts for temperature-independent apparent formation factors for 4.4–87.6 ppt salinities, while a clay-conduction model more successfully accounts for temperature-dependent apparent formation factors at 1.2 ppt. Both mechanisms account for some correlation of C_w/C_o with porosity at low fluid conductivities; neither accounts for the surprising strengths of these correlations. The lack of correlation between measured CEC values and those predicted on the basis of equation 1 is difficult to reconcile with a clay-conduction model.

The possibility of microcrack conduction in our basalts does not imply that microcracks are a viable general alternative to clay conduction for other rock types. Clay conduction is certainly more likely in most shales, and the basalt conductivity studies of Olhoeft (1977, 1981) and Karato (1985) imply activation energies more consistent with clay than with seawater. Thus clay-surface conduction remains as the most plausible general mechanism for C_w-independent sample conductivity, but the possible role of microcracks warrants further study.

ACKNOWLEDGMENTS

We thank M. Batzle, D. Morgan, and P. Pezard for their advice concerning resistivity measurement techniques. We thank Morton J. Ridge for advice concerning measurement of cation exchange capacity. This project was made possible by the U.S. Science Advisory Committee, grant TAMRF P.O. 20326.

The U.S. Science Program associated with the Ocean Drilling Program is sponsored by the National Science Foundation and the Joint Oceanographic Institutions, Inc. Any opinions, findings and conclusions expressed in this publication are those of the authors and do not necessarily reflect the views of the National Science Foundation, the Joint Oceanographic Institutions, Inc., Texas A&M University, or Columbia University.

REFERENCES

Adamson, A. C., 1979. Chemistry of alteration minerals from DSDP Sites 501, 504, and 505. *In* Cann, J. R., Langseth, M. G., Honnorez, J., Von Herzen, R. P., White, S. M., et al., *Init. Repts. DSDP,* 69: Washington (U.S. Govt. Printing Office), 551–564.

_____, 1985. Basement lithostratigraphy, DSDP Hole 504B. *In* Anderson, R. N., Honnorez, J., Becker, K., et al., *Init. Repts. DSDP,* 83: Washington (U.S. Govt. Printing Office), 121–127.

Alt, J. C., and Emmermann, R., 1985. Geochemistry of hydrothermally altered basalts: DSDP Hole 504B. *In* Anderson, R. N., Honnorez, J., Becker, K., et al., *Init. Repts. DSDP,* 83: Washington (U.S. Govt. Printing Office), 249–262.

Alt, J. C., Honnorez, J., Laverne, C., and Emmermann, R., 1986. Hydrothermal alteration of a 1 km section through the upper oceanic crust, Deep Sea Drilling Project Hole 504B: mineralogy, chemistry, and evolution of seawater-basalt interactions. *J. Geophys. Res.,* 91:10309–10335.

Anderson, R. N., Zoback, M. D., Hickman, S. H., and Newmark, R. L., 1985. Permeability versus depth in the upper oceanic crust: in situ measurements in DSDP Hole 504B, eastern equatorial Pacific. *J. Geophys. Res.,* 90:3659–3669.

Archie, G. E., 1942. The electrical resistivity log as an aid in determining some reservoir characteristics. *J. Pet. Tech.,* 5:1–8.

Becker, K., 1985. Large-scale electrical resistivity and bulk porosity of the oceanic crust, Deep Sea Drilling Project Hole 504B, Costa Rica Rift. *In* Anderson, R. N., Honnorez, J., Becker, K., et al., *Init. Repts. DSDP,* 83: Washington (U.S. Govt. Printing Office), 419–427.

_____, 1989. Measurements of the permeability of the sheeted dikes in Hole 504B, ODP Leg 111. *In* Becker, K., Sakai, H., et al., *Proc. ODP, Sci. Results,* 111: College Station, TX (Ocean Drilling Program), 317–325.

Ellis, D. V., 1987. *Well Logging for Earth Scientists:* New York (Elsevier).

Flovenz, O. G., Georgsson, L. S., and Arnason, K., 1985. Resistivity structure of the upper crust in Iceland. *J. Geophys. Res.,* 90:10136–10150.

Karato, S. I., 1985. Physical properties of basalts from the Galapagos, Leg 70. *In* Cann, J. R., Langseth, M. G., Honnorez, J., Von Herzen, R. P., White, S. M., et al., *Init. Repts. DSDP,* 69:423–428.

Matijevic, E., 1974. *Surface and Colloid Science* (Vol. 7): New York (Wiley).

Olhoeft, G. R., 1977. Electrical properties of water-saturated basalts, preliminary results to 506°K (233°C), *Open File Rep.–U.S. Geol. Surv.,* 77:688.

_____, 1981. Electrical properties of rocks. *In* Touloukian, Y. S., Judd, W. R., and Roy, R. F., *Physical Properties of Rocks and Minerals:* New York (McGraw Hill), 257–330.

Pape, H., Riepe, L., and Schopper, J. R., 1982. Petrophysical detection of microfissures in granites. *SPWLA 26th Ann. Log Symp.,* Dallas, TX, Paper P.

Pezard, P. A., 1990. Electrical properties of mid-ocean ridge basalt and implications for the structure of the upper oceanic crust in Hole 504B. *J. Geophys. Res.,* 95:9237–9264.

Pezard, P. A., and Anderson, R. N., 1989. Morphology and alteration of the upper oceanic crust from *in-situ* electrical experiments in DSDP/ODP Hole 504B. *In* Becker, K., Sakai, H., et al., *Proc. ODP, Sci. Results,* 111: College Station, TX (Ocean Drilling Program), 133–146.

Rangin, C., Silver, E. A., von Breymann, M. T., et al., 1990. *Proc. ODP, Init. Repts.,* 124: College Station, TX (Ocean Drilling Program).

Ridge, M. J., 1983. A combustion method for measuring the cation exchange capacity of clay minerals. *Log Analyst,* 24:6–11.

Serra, O., 1984. *Fundamentals of Well-Log Interpretation:* Amsterdam (Elsevier).

Shipboard Scientific Party, 1990. Explanatory notes. *In* Rangin, C., Silver, E. A., von Breymann, M. T., et al., *Proc. ODP, Init. Repts.,* 124: College Station, TX (Ocean Drilling Program), 7–33.

Waxman, M. H., and Smits, L.J.M., 1968. Electrical conductivities in oil-bearing shaly sands. *Trans. AIME,* 243.

Weissel, J. K., 1980. Evidence for Eocene oceanic crust in the Celebes Basin. *In* Hayes, D. E. (Ed.), *The Tectonic and Geologic Evolution of Southeast Asian Seas and Islands.* Am. Geophys. Union, Geophys. Monogr. Ser., 23:37–47.

Wilkens, R., Schultz, D., and Carlson, R., 1988. Relationship of resistivity, velocity, and porosity for basalts from downhole well-logging measurements in Hole 418A. *In* Salisbury, M. H., Scott, J. H., et al., *Proc. ODP, Sci. Results,* 102: College Station, TX (Ocean Drilling Program), 69–75.

Winsauer, W. O., and McCardell, W. M., 1953. Ionic double-layer conductivity in reservoir rocks. *Petrol. Trans. AIME,* 198:129–134.

Date of initial receipt: 2 July 1990
Date of acceptance: 17 June 1991
Ms 124B-172